TNF-α over-expression in lung disease: a single cause behind a complex phenotype

Lennart KA Lundblad, John Thompson-Figueroa, Timothy Leclair, Michael J Sullivan, Matthew E Poynter, Charles G Irvin and Jason HT Bates

On-line data supplement

Methods

Animals. SP-C/TNF-α transgenic mice (TG+) were obtained by backcrossing heterozygous male transgenic mice with wild type C57BL/6 female mice to generate heterozygous offspring. The TG+ has been maintained as a heterozygous line by repeated backcrossing in our facility since 2001. We studied female mice aged 7 – 11 months of age. Littermate transgene-negative mice (control) served as controls, since we believe that these animals are the most closely matched both from a genetical and age point of view. The animal weights were not significantly different between groups (23.25 ± 0.69 g and 24.75 ± 1.14 g in TG+ and controls respectively). The mice were bred in our animal facility with free access to food and water. A sentinel animal program ensured that the animals were free of common pathogens for this species. The Institutional Animal Care and Use Committee of the University of Vermont approved the experiments.

Genotyping. We identified transgenic mice by PCR analysis of genomic DNA isolated from small tissue samples obtained by ear punching. The PCR method has been explained extensively elsewhere (E1). Briefly, SP-C/TNF-α transgenic mice were identified by PCR amplification of genomic DNA isolated from the ear biopsies, using a forward primer within the SP-C promoter (5'-agatatgtgggaggaggcaa-3') and a reverse primer within TNFα (5'-gagaagagggtgagacatag-3'), generating an 800bp amplicon. As an internal PCR control, genomic DNA was PCR amplified using primers within the myosin heavy chain gene, forward (5'-gaggagcgggctgacatc-3'), reverse (5'-acccagagaggcaagtgacc-3'), generating a 180bp amplicon. PCR products were resolved on 1% agarose gels containing ethidium bromide and visualized under UV light.

Animal preparation. We studied TG+ transgenic mice (n = 10) and littermate controls (n = 10). The mice were anesthetized by intra-peritoneal injection of sodium pentobarbital (90 mg/kg), and the trachea was dissected free of surrounding tissue and cannulated with an 18-gauge cannula. The mice were then installed in a custom-designed whole body plethysmograph and connected to a small animal ventilator (*flexiVent*, SCIREQ, Montreal, Canada), as previously described (E2). Positive end-expiratory pressure (PEEP) was achieved by submerging the exhalation port of the *flexiVent* under water. Once ventilation was initiated (200 breaths/minute, tidal volume 0.20 ml), the mice were paralyzed with intra-peritoneal pancuronium (0.8μg/kg). An ECG monitor (Silogic Ltd. United Kingdom) was connected via subcutaneous needles to the four limbs of the mice to determine heart rate as a monitor of depth of anesthesia.

Determination of input impedance: To measure the *Zrs*, we applied a 2 s broad-band volume perturbation signal to the lungs with the *flexiVent*. The volume signal consisted of the superposition of 13 sine waves having frequencies spaced roughly evenly over the range 1 Hz to 20.5 Hz. *Zrs* was calculated from the displacement of the ventilator piston and the pressure in the ventilator cylinder as described previously (E3, E4). Correction for gas compressibility as well as resistive and accelerative losses in the *flexiVent*, connecting tubing and the tracheal cannula were performed as described previously (E5) using dynamic calibration data obtained by applying volume perturbations through the tubing and tracheal cannula first when it was completely closed and then when it was open to the atmosphere. We interpreted the measurement of *Zrs* in terms of the constant phase model (E6)

$$Zrs(f) = Rn + i2\pi fIaw + \frac{G - iH}{(2\pi f)^{\alpha}} \qquad (1)$$

where *Rn* is the frequency independent Newtonian resistance reflecting that of the conducting airways, *Iaw* is airway gas inertance, *G* characterizes tissue resistance, *H* characterizes tissue stiffness, *i* is the imaginary unit, α links *G* and *H*, and *f* is frequency in Hz. A quantity known as hysteresivity (η=G/H) was also calculated; η tends to increase when regional heterogeneity in the lung develops (E6, E7).

Analysis of pressure-volume loops: Quasi-static *PV* loops were obtained, starting at functional residual capacity as defined by each level of PEEP, by inflating the lungs in seven 0.1 ml steps and then deflating them again in the same seven steps, pausing at each step for 1 s. The plateau in *P* at each step was related to the total volume delivered (E8). The shape factor (*k*) of the descending limb of the *PV* loop was calculated by fitting the data to the Salazar-Knowles equation,

$$V = A - Be^{-kP_{ao}} \qquad (2)$$

where *V* is the volume, *A* and *B* are constants, and P_{ao} is the airway opening pressure. The value of the parameter *k* is thought to change characteristically with both fibrosis and emphysema (E9, E10).

Measurement of thoracic gas volume: V_{TG} was measured and calculated as described previously (E2, E11). Briefly, a rotating shaft was sealed through the rear face of the plethysmograph. Rotating the shaft from outside the chamber caused a paddle connected to the inside end of the shaft to compress the chest of the mouse while it was inside the plethysmograph. We recorded the resulting pressure changes inside the plethysmograph (P_b) and at the airway opening (P_{ao}) while cyclically compressing the chest during periods of apnea at functional residual capacity. Following correction of P_b for thermal artifacts inside the plethysmograph, we calculated V_{TG}, on

the basis of Boyle's law, from the elastance of the air in the plethysmograph and the slope of P_b versus P_{ao} measured during the cyclic chest compressions.

Micro-computed tomography: The euthanized mouse was placed in a GE Medical Systems eXplore RS80 Laboratory volumetric cone-beam micro-CT scanner and scanned at 80 kVp, 450 mAs, 720 views for 80 min. Volumes were reconstructed from the scan data at a resolution of 0.047 mm per voxel side. A number of the mice were not successfully scanned due to motion artifacts. Consequently, the micro-CT lung and chest volumes reported are based on a subset of the animals studied (n = 7 for TG+ and n = 6 for controls).

Lung volumes – CT: Lung volumes were calculated using Microview visualization software, version 1.2.0-b2 (GE HealthCare, London, ON, Canada). Two-dimensional Regions of Interest (2D ROIs) were created on approximately 10 cross-sectional images selected from a range of slices between the proximal end of the trachea and the base of the lungs. The 2D ROIs were defined by freehand contours drawn to closely surround the lungs and trachea so that all extrathoracic gas (e.g. bowel gas immediately below the diaphragm and ambient air outside the body) was excluded. 2D ROIs were then automatically created for all cross-sections by linear interpolation between the manually drawn contours, and 3D ROIs were subsequently generated by stacking each set of 2D regions. Frequency histograms of Hounsfield Units (HU) were calculated for the voxels contained within each 3D ROI. The frequencies of the HUs between -1000 and 0 (corresponding to air and water, respectively) were then converted to fraction of air by multiplying each frequency by its HU and then dividing by -1000. These fractions were then summed and multiplied by the voxel volume of 1.038×10^{-7} ml to yield an estimate for V_{TG}.

Thoracic volume – CT: Estimates of thoracic volume were obtained by counting the voxels contained within a 3D ROI generated by a method similar to that described above. We used elliptical contours drawn to fit closely inside the area bounded by the sternum, ribs and vertebra on 4 cross-sectional images selected from a range of slices between the apex and base of the lungs. The voxel counts were converted to ml multiplication by the voxel volume (1.038×10^{-7} ml).

CT – renderings: Isosurface renderings of the lung were created using an algorithm in the Microview software that draws a 3D surface over all voxels having grayscale values at or above a given threshold. Image data were inverted so that the upper limit of the grayscale range represented the lowest X-ray attenuation. A threshold value corresponding to approximately -500 HU in non-inverted data was selected so that the spaces enclosed by the surface were considered to be occupied by at least 50% air. The resulting isosurface rendering was thus a virtual cast of the air contained within the airways and parenchyma (Fig. E2).

Maximum Intensity Projection (MIP): MIP images were generated from inverted image data, where the maximum intensities represent air. The MIP image is produced by casting parallel rays through the image along the Y-axis. Each output pixel in the MIP image represents the maximum intensity value found along the corresponding ray cast through the original image

Histological analysis: When the micro-CT scan was completed, the chest was opened and the lungs and heart excised *in toto*. The trachea was re-cannulated and the lungs inflated to 30 cmH_2O by intra-tracheal instillation of 10% neutral buffered formalin (Accustain, Sigma Aldrich). The trachea was tied off and the lungs were immersed in the same buffer overnight and then soaked in 70% ethanol. The lung was then embedded in paraffin and cut with a

microtome at 10 μm and mounted on glass slides, and stained with hematoxylin and eosin (H&E stain). A second set of slides were stained with Sirius Red and Fast Green FCF, and observed under polarized light microscopy for collagen visualization at 100 x magnification as described elsewhere (E12, E13). The slides were masked, and then read and scored independently by two experienced technicians, not otherwise involved in the study. The scoring was repeated twice three days apart and the average score calculated. The slides received a score of either 1, 2 or 3, where 1 corresponded to the least amount of collagen staining and 3 the most intense/organized staining. The between-reader scores and between-day scores were not significantly different.

One slide was chosen randomly from each lung. From each of these slides we selected five 872.3 μm × 691.1 μm regions, each containing a major airway, for imaging at a resolution of 0.671 μm/pixel. We quantified the size of open airspaces in each image using a technique we developed that is essentially an extension of the mean linear intercept technique previously described by Soutiere et al. (E14). Our analysis was implemented in a Java Plugin for the NIH ImageJ software (version 1.34a) (E15), and performs the following sequence of operations. First, a number of pre-processing steps have to be performed to convert the 8-bit gray-scale image to a black&white image. This begins with all pixels above an optimal threshold (E16) being converted to black (tissue) and the remainder being converted to white (air). The result is usually not a perfectly clean black&white image, however, because noise in the original gray-scale image causes white speckles to appear in what should be purely black regions. These are eliminated by a dilation process in which all white pixels adjacent to a black pixel are converted to black pixels. We apply this dilation process three times in succession in order to eliminate white speckles larger than a single pixel. We have found that this produces clean images of a black tissue network superimposed on a white background of air.

Next, the airspace structure in the pre-processed black&white image is analyzed as follows. First, each row of pixels in the image is examined for runs of contiguous white pixels, excluding those runs that either begin or terminate at the edge of the image. The length of each run corresponds to the horizontal distance across the airspace it traverses. We then construct a length-weighted histogram by counting the number of times each run length occurs in the image, multiplying this number by the length itself (in μm), and plotting the result against length (see Fig. 7 of the main manuscript). Finally, the centroid of the histogram (L_c) is calculated as a reflection of the mean airspace dimension in the image.

Note that we base our analysis on the length-weighted histogram of lengths rather than simply the histogram of lengths for the following reason. Suppose, for example, that an image is composed of a network of tissue surrounding a collection of square airspaces, and that half the image contains airspaces that are a distance l across while the remaining half contains larger airspaces that are $2l$ across (Fig. E1A). The histogram of lengths of horizontal runs of white pixel for this image is zero everywhere except for the lengths l and $2l$. Furthermore, because there are four times as many small airspaces as large ones, the height of the histogram at l is four times that at $2l$ (Fig. E1B). The value of the histogram at these two positions thus does not reflect the relative areas of the images composed of small and large airspaces. Instead, it is unfairly weighted toward the small airspaces simply because more of them can be fit into a given image area. To rectify this situation, we multiply each vertical value in the histogram by its corresponding length. This makes the two spikes in the present example equal in height (Fig. E1C), as is appropriate for the relative proportions of the image they represent.

Statistics: Data are presented as means ± SEM. *Zrs*, V_{TG} and k data were compared using one-way ANOVA. Body weights and L_c were compared using a two-sample independent T-test.

Histological scores were compared using a Wilcoxon rank-sum test. P values smaller than 0.05 were taken as significant.

References

E1. Miyazaki, Y., K. Araki, C. Vesin, I. Garcia, Y. Kapanci, J. A. Whitsett, P. F. Piguet, and P. Vassalli. 1995. Expression of a tumor necrosis factor-alpha transgene in murine lung causes lymphocytic and fibrosing alveolitis. A mouse model of progressive pulmonary fibrosis. *J Clin Invest* 96(1):250-9.

E2. Lundblad, K. A. L., J. Thompson-Figueroa, T. Leclair, C. G. Irvin, and J. H. T. Bates. 2004. Thoracic gas volume measurements in paralyzed mice. *Ann Biomed Eng* 32(10):1420-1427.

E3. Gomes, R. F., X. Shen, R. Ramchandani, R. S. Tepper, and J. H. Bates. 2000. Comparative respiratory system mechanics in rodents. *J Appl Physiol* 89(3):908-16.

E4. Hirai, T., K. A. McKeown, R. F. Gomes, and J. H. Bates. 1999. Effects of lung volume on lung and chest wall mechanics in rats. *J Appl Physiol* 86(1):16-21.

E5. Tomioka, S., J. H. Bates, and C. G. Irvin. 2002. Airway and tissue mechanics in a murine model of asthma: alveolar capsule vs. forced oscillations. *J Appl Physiol* 93(1):263-70.

E6. Hantos, Z., B. Daroczy, B. Suki, S. Nagy, and J. J. Fredberg. 1992. Input impedance and peripheral inhomogeneity of dog lungs. *J Appl Physiol* 72(1):168-78.

E7. Schuessler, T., and J. Bates. 1995. A computer-controlled research ventilator for small animals: design and evaluation. *IEEE Trans Biomed Eng* 42(9):860-866.

E8. Wagers, S., L. Lundblad, H. T. Moriya, J. H. Bates, and C. G. Irvin. 2002. Nonlinearity of respiratory mechanics during bronchoconstriction in mice with airway inflammation. *J Appl Physiol* 92(5):1802-1807.

E9. Colebatch, H. J., I. A. Greaves, and C. K. Ng. 1979. Exponential analysis of elastic recoil and aging in healthy males and females. *J Appl Physiol* 47(4):683-91.

E10. Colebatch, H. J., C. K. Ng, and N. Nikov. 1979. Use of an exponential function for elastic recoil. *J Appl Physiol* 46(2):387-93.

E11. Lundblad, L. K. A., C. G. Irvin, A. Adler, and J. H. Bates. 2002. A reevaluation of the validity of unrestrained plethysmography in mice. *J Appl Physiol* 93(4):1198-207.

E12. Junqueira, L. C., G. Bignolas, and R. R. Brentani. 1979. Picrosirius staining plus polarization microscopy, a specific method for collagen detection in tissue sections. *Histochem J* 11(4):447-55.

E13. Junquiera, L. C., L. C. Junqueira, and R. R. Brentani. 1979. A simple and sensitive method for the quantitative estimation of collagen. *Anal Biochem* 94(1):96-9.

E14. Soutiere, S. E., Tankersley, C.G., Mitzner, W. 2004. Differences in alveolar size in inbred mouse strains. *Respiratory Physiology & Neurobiology* 140(3):283-291.

E15. Rasband, W. S. 1997-2004. ImageJ, http://rsb.info.nih.gov/ij/. National Institutes of Health.

E16. Ridler, T. W., and S. Calvard. 1978. Picture thresholding using an iterative selection method. *IEEE Transactions on Systems, Man and Cybernetics* SMC-8(8):630.

Figure E1: A) A black & white image composed of half large airspaces (linear dimension 2*l*) and half small airspaces (linear dimension *l*). B) Histogram of horizontal lengths of runs of contiguous white pixels in the image. C) Length-weighted histogram of lengths of white pixel runs.

Fig. E1

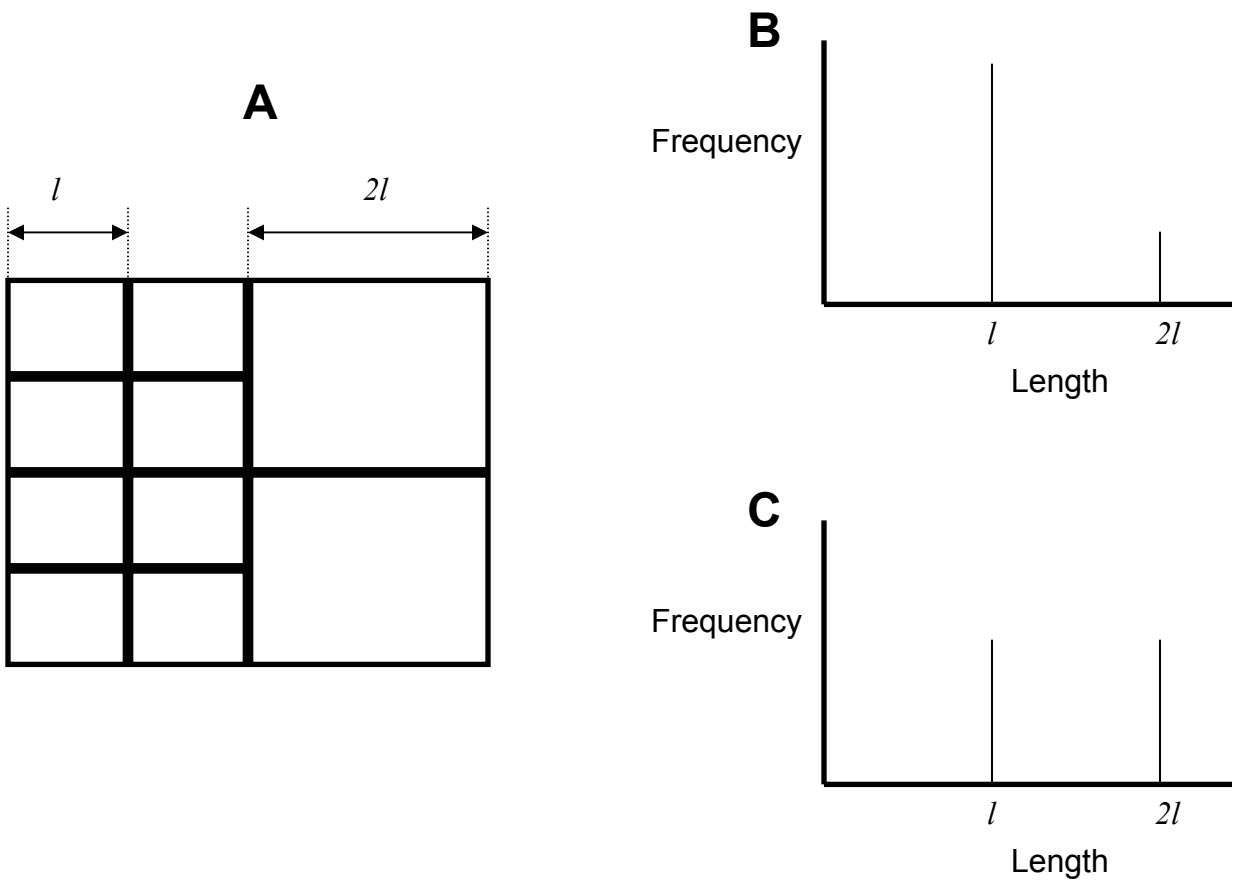

Figure E2: Movie clips of iso-surface renderings showing the entire lung from a control mouse (A) and a TG+ mouse (B). These images represent the interface between air and tissue in the lung. In the control lung (A) the interface is smooth, and indentations from the ribs are clearly visible. By contrast, the air-tissue interface of the TG+ lung (B) is rough with a nodular appearance. This is due to patchy consolidation of the parenchyma, and reveals some intra-lobar airways that are not visible in the control lung. Please view associated movie files.

A **B**